Research Square

Preprints are preliminary reports that have not undergone peer review.
They should not be considered conclusive, used to inform clinical practice,
or referenced by the media as validated information.

KDM5B drives acute liver injury by impairing autophagy and activating cGAS-STING signaling via binding to ATG16L1

Lihua Qu

lihuaqu@whu.edu.cn

Wuhan University, https://orcid.org/0009-0008-2157-4659

Haoxiang Ou

Hubei University of Science and Technology

Yaoyao Ma

Hubei University of Science and Technology

Jiangyue Wang

Hubei University of Science and Technology

Jiaqi Xiao

Hubei University of Science and Technology

Danxia Liu

Hubei University of Science and Technology

Yongfen Bao

Hubei University of Science and Technology

Shigang Shan

Hubei University of Science and Technology

Qing Yao

Hubei University of Science and Technology

Wentao Huang

Hunan Normal University School of Medicine

Xinyu Que

Hubei University of Science and Technology

Xuan Qin

Hubei University of Science and Technology

Chao Chen

Nanjing University of Chinese Medicine

Article

Keywords: Acute liver injury, Inflammation, Autophagy, KDM5B, cGAS-STING

Posted Date: September 12th, 2025

DOI: https://doi.org/10.21203/rs.3.rs-7430149/v1

License: This work is licensed under a Creative Commons Attribution 4.0 International License.
Read Full License

Additional Declarations: (Not answered)

Abstract

Acute liver injury (ALI) is a severe hepatic disorder characterized by high morbidity and mortality, presenting major challenges for clinical management. However, its underlying pathogenesis remains incompletely understood. Through analysis of four Gene Expression Omnibus (GEO) datasets using the Robust Rank Aggregation (RRA) method and RNA sequencing, the histone demethylase KDM5B was identified as a core upregulated gene in ALI. This finding was validated in carbon tetrachloride (CCl_4)-induced murine ALI models, in which KDM5B expression was significantly elevated. Liver-specific knockdown of KDM5B via AAV-shKDM5B alleviated hepatic injury by reducing immune cell infiltration and inflammatory cytokine release, while enhancing autophagic flux. Mechanistically, KDM5B bound to the autophagy-related protein ATG16L1, disrupting the assembly of the ATG12-ATG5-ATG16L1 complex and impairing autophagosome maturation. This led to the accumulation of cytoplasmic DNA, which activated the cGAS-STING-TBK1-IRF3/NF-κB signaling pathway and amplified pro-inflammatory responses. This study revealed a protein-interaction-dependent mechanism by which KDM5B inhibited autophagy and triggered cGAS-STING signaling. It uncovered a novel mechanism underlying the vicious cycle of impaired autophagy and excessive inflammation in ALI, offering a molecular basis and potential therapeutic target involving the KDM5B-ATG16L1 axis.

Introduction

Acute liver injury (ALI) is a common disorder that poses a significant threat to public health [1]. Its pathogenesis is complex, marked by a sudden onset and progressive deterioration. Critically, ALI often serves as the precursor to acute liver failure and can rapidly progress to liver failure [2], which triggering systemic inflammatory responses, coagulopathy, multi-organ dysfunction, and potentially life-threatening conditions [3, 4]. Notably, ALI can be induced by various etiological factors, such as viral infections (e.g., hepatitis B and C viruses), drug or toxin exposure (e.g., acetaminophen overdose) and autoimmune reactions [5, 6, 7, 8]. Current therapeutic approaches primarily include pharmacological treatments, supportive care, and liver transplantation [9]. However, the scarcity of donor organs [10], suboptimal efficacy of existing pharmacotherapies [11], and an incomplete understanding of the underlying pathogenesis in many cases continue to hinder clinical management. Therefore, further investigation into the mechanisms driving ALI and the identification of novel therapeutic targets is urgently needed.

Autophagy is an evolutionarily conserved lysosomal degradation pathway in eukaryotes that maintains cellular homeostasis and metabolic stability [12]. To date, at least 19 autophagy-related proteins have been identified as essential regulators of autophagosome formation. Initially discovered in yeast, these proteins are highly conserved across eukaryotic species [13]. During autophagy initiation, microtubule-associated protein 1 light chain 3 (LC3) and the ATG12-ATG5-ATG16L1 complex assemble on the phagophore. Interacting with the ATG12-ATG5 conjugate, ATG16L1 forms a dimeric complex that activates ATG3, thereby promoting the lipidation of LC3 with phosphatidylethanolamine. This process converts LC3B-I to LC3B-II, which is essential for autophagy activation [14]. Thus, the formation of the

ATG12-ATG5-ATG16L1 complex is essential for autophagosome maturation. In the context of ALI, autophagy plays a dual role: homeostatic autophagy helps to eliminate damaged organelles and misfolded proteins, while dysregulated autophagy amplifies inflammation and induces cell death [15]. For example, macrophage-specific deletion of ATG16L1 in partial hepatectomy models reduces autophagic flux, activates inflammatory pathways, and impairs liver regeneration [16]. Similarly, hepatocyte-specific knockdown of ATG5 blocks autophagosome formation and aggravates lipopolysaccharide (LPS)-induced hepatic inflammation [17]. These findings highlight the essential anti-inflammatory role of autophagy [18, 19]. However, the molecular mechanisms underlying autophagy dysregulation in ALI remain poorly understood and warrant further investigation.

The cyclic GMP-AMP synthase–stimulator of interferon genes (cGAS-STING) pathway is a key innate immune signaling axis that has garnered considerable attention in recent years [20]. Its functions by sensing aberrant cytosolic DNA and initiating inflammatory responses [21]. Within this pathway, cGAS serves as the cytosolic DNA sensor. Upon detecting and binding to cytosolic DNA, cGAS catalyzes the production of the second messenger 2'3'-cyclic GMP-AMP (cGAMP). Subsequently, cGAMP binds to and activates the STING, which is located on the endoplasmic reticulum membrane [22, 23]. Upon activation, STING undergoes a conformational change and recruits TANK-binding kinase 1 (TBK1), which phosphorylates interferon regulatory factor 3 (IRF3). This leads to the production of type I interferons (IFN-I) and pro-inflammatory cytokines like tumor necrosis factor-alpha (TNF-α) and interleukin-6 (IL-6) [24]. Dysregulated cGAS-STING signaling contributes to immunopathology in various hepatic inflammatory diseases [25]. In ALI, activation of this pathway promotes inflammatory cell infiltration and hepatocyte apoptosis [26]. Although the pro-inflammatory role of cGAS-STING signaling in ALI is well established [26], the upstream molecular events leading to its activation remain incompletely understood.

Lysine Demethylase 5B (KDM5B), a member of the Jumonji C (JmjC) domain-containing histone demethylase family, is best known for catalyzing the demethylation of histone H3 lysine 4 di- and tri-methylation (H3K4me2/3), thereby modulating transcriptional activity [27]. However, the function of KDM5B extends beyond histone demethylation. For example, a study in alcohol-exposed male mice showed that KDM5B can bind to the promoter region of hepatocyte nuclear factor 4 alpha (HNF4A) and exacerbate alcohol-induced hepatocyte injury through a mechanism independent of its histone demethylase function [28]. While KDM5B has been implicated in tumorigenesis, stem cell differentiation, and metabolic disorders [29, 30], its specific role and underlying mechanisms in the context of ALI remain unexplored.

In this study, we found that KDM5B binds to the key autophagy-related protein ATG16L1, disrupting the formation of the ATG12-ATG5-ATG16L1 complex and thereby inhibiting autophagosome maturation in ALI. This autophagy impairment resulted in the accumulation of cytosolic DNA, which activated the cGAS-STING signaling pathway and triggered excessive inflammatory cytokine release, ultimately exacerbating hepatic injury. To validate this mechanism, we generated a hepatocyte-specific KDM5B knockdown mouse model. KDM5B knockdown significantly alleviated carbon tetrachloride (CCl_4)-

induced ALI, as evidenced by reduced immune cell infiltration, restoration of autophagic flux, and suppression of cGAS-STING pathway activation. Collectively, these findings uncovered a novel mechanism by which KDM5B regulated autophagy independently of its histone demethylase activity, providing a theoretical basis for targeting the KDM5B-ATG16L1 axis as a potential therapeutic strategy for ALI.

Results

GEO dataset-based differential gene expression analysis in ALI

To identify potential genes related to ALI, we analyzed four Gene Expression Omnibus (GEO) datasets and identified 400 differentially expressed genes (DEGs). Robust Rank Aggregation (RRA) analysis further narrowed this to 40 significantly altered genes, including 20 upregulated and 20 downregulated genes. Notably, KDM5B was markedly upregulated in ALI patients compared to controls (Fig. 1A-B). Additionally, Kyoto Encyclopedia of Genes and Genomes (KEGG) enrichment analysis showed enriched DEGs in innate immune and inflammatory pathways, including the cytosolic DNA-sensing pathway and the interleukin-17 (IL-17) signaling pathway (Fig. 1C).

KDM5B expression was significantly up-regulated in ALI

To validate KDM5B as a key DEG in ALI, we established a murine model via intraperitoneal injection of CCl_4 and performed RNA sequencing on liver tissues collected 24 hours post-injection (Fig. 2A). Volcano plot analysis identified 1,084 DEGs compared to controls, including 733 upregulated and 351 downregulated genes (Fig. 2B). Heatmap analysis of the KDM family revealed a marked upregulation of KDM5B in CCl_4-treated mice (Fig. 2C), which was further confirmed by quantitative real-time PCR (qRT-PCR), showing significantly elevated KDM5B mRNA levels in CCl_4-induced liver tissues (Fig. 2D). To further assess KDM5B protein expression, immunohistochemistry and western blotting were performed on liver tissues collected at 24 and 48 hours after CCl_4 injection. Immunohistochemical staining showed a significant increase in KDM5B expression at 24 hours, followed by a decline at 48 hours (Fig. 2E). Consistently, western blotting revealed a similar pattern, with peak KDM5B expression at 24 hours and a relative decrease at 48 hours compared to the controls (Fig. 2F). To investigate KDM5B expression in different liver cell types, we isolated primary hepatocytes, lymphocytes, and macrophages from CCl_4-treated mice. The qRT-PCR analysis showed that KDM5B expression was markedly elevated in all three cell types following CCl_4 administration (Fig. 2G). Collectively, the findings indicate that both KDM5B mRNA and protein levels are significantly upregulated in CCl_4-induced murine model of ALI.

Liver-specific knockdown of KDM5B ameliorated CCl-induced ALI

To explore the functional role of KDM5B in CCl_4-induced ALI, we administered adeno-associated virus (AAV) vectors encoding either shRNA targeting KDM5B (AAV-shKDM5B) or KDM5B overexpression construct (AAV8-KDM5B) via tail vein injection. Two weeks post-injection, ALI was induced through intraperitoneal administration of CCl_4 (1 mL/kg), and liver tissues were collected 24 hours later for analysis (Fig. 3A). Hematoxylin and eosin (H&E) staining revealed a significant reduction in necrotic liver areas in mice with liver-specific KDM5B knockdown compared to control groups (Fig. 3B). Correspondingly, serum levels of alanine aminotransferase (ALT) and aspartate aminotransferase (AST), both indicators of liver injury, were significantly decreased in the knockdown group (Fig. 3C). Western blot analysis confirmed that AAV-shKDM5B effectively reduced hepatic KDM5B protein expression in CCl_4-treated mice, indicating successful knockdown of KDM5B (Fig. 3D). In contrast, liver-specific overexpression of KDM5B aggravated liver injury. H&E staining showed significantly enlarged necrotic areas (Fig. 3E), accompanied by a marked increase in serum ALT and AST levels compared to controls (Fig. 3F). Collectively, these findings demonstrate the critical role of KDM5B in the pathogenesis of CCl_4-induced ALI. Liver-specific knockdown of KDM5B significantly mitigates liver injury, whereas its overexpression exacerbates hepatic damage.

Liver-specific knockdown of KDM5B alleviated inflammation in CCl-induced ALI

To examine the immunoregulatory role of KDM5B in CCl_4-induced ALI, the impact of KDM5B modulation on hepatic inflammatory responses was assessed. Immunohistochemical staining revealed that CCl_4 treatment significantly increased infiltration of $F4/80^+$ macrophages in the liver, which was markedly reduced by AAV-shKDM5B treatment. Conversely, AAV8-KDM5B overexpression further intensified macrophage infiltration (Fig. 4A). Additionally, CCl_4 treatment markedly increased hepatic mRNA expression of pro-inflammatory cytokines (IL-6, IL-1β, IL-18, as well as TNF-α), the chemokine CXCL10, and interferon-stimulated genes (ISG15 and IFN-β). These increases were significantly suppressed in the AAV-shKDM5B group (Fig. 4B-H). In contrast, AAV8-KDM5B treatment elevated the transcription of these inflammatory mediators (Fig. 4I-L). Consistent with the mRNA data, enzyme-linked immunosorbent assay (ELISA) showed obviously decreased serum levels of pro-inflammatory cytokines in the KDM5B knockdown group (Fig. 4M-P). Flow cytometry analysis further confirmed a decreased proportion of hepatic $CD11b^+F4/80^+$ macrophages in the KDM5B knockdown group (Fig. 4Q). Collectively, these findings demonstrate that KDM5B promotes immune cell infiltration and upregulation of inflammatory mediators, thereby contributing to the pathogenesis of ALI.

KDM5B promoted the pathological process of ALI by inhibiting autophagy

Given the pivotal role of autophagy in ALI, we further explored whether KDM5B modulates autophagic activity. AML12 hepatocytes were transfected with shKDM5B plasmids to knock down KDM5B

expression, followed by LPS treatment to induce stress. Autophagy-related markers were then assessed. qRT-PCR and western blotting revealed that LPS exposure significantly reduced the mRNA and protein levels of autophagy markers LC3-II/LC3-I and Beclin-1, while increasing the accumulation of the selective autophagy substrate p62/SQSTM1, indicating impaired autophagic flux. Notably, KDM5B knockdown effectively rescued LPS-induced autophagy inhibition, as evidenced by restored LC3-II/LC3-I and Beclin-1 expression and reduced p62/SQSTM1 levels (Fig. 5A-D). Supporting these findings, transmission electron microscopy (TEM) showed a significant decrease in autophagosome numbers following LPS treatment, whereas KDM5B knockdown markedly increased autophagosome formation (Fig. 5E). Confocal microscopy further corroborated these results, demonstrating diminished LC3 puncta formation in LPS-treated cells, which was significantly enhanced upon KDM5B knockdown (Fig. 5F). Collectively, these findings indicate that KDM5B knockdown restores autophagic activity, suggesting that KDM5B contributes to ALI pathogenesis through inhibition of autophagy.

KDM5B binding to ATG16L1 inhibited ATG12-ATG5-ATG16L1 complex formation and impaired autophagy in ALI

To explore the potential molecular mechanism by which KDM5B suppressed the autophagy in ALI, we transfected AML12 hepatocytes with a Flag-tagged KDM5B expression plasmid. Flag-KDM5B was immunoprecipitated, and interacting proteins were identified via liquid chromatography-tandem mass spectrometry (LC-MS/MS) (Fig. 6A). Silver staining confirmed efficient expression and purification of Flag-KDM5B (Fig. 6B). Bioinformatic analysis using the STRING database predicted a potential interaction between KDM5B and ATG16L1 (Fig. 6C). Consistently, LC-MS/MS analysis identified ATG16L1 as one of the KDM5B-interacting proteins (Fig. 6D). To validate this interaction, co-immunoprecipitation (Co-IP) assays were performed, confirming that KDM5B physically binds to ATG16L1 (Fig. 6E-F). Additionally, confocal microscopy revealed strong spatial co-localization between KDM5B and ATG16L1 (Fig. 6G). Further experiments demonstrated that overexpression of KDM5B significantly disrupted the interaction of ATG16L1 with the ATG12-ATG5 complex (Fig. 6H), which is essential for autophagosome maturation. Moreover, ATG16L1 knockdown significantly reduced the LC3-II/LC3-I ratio, further confirming the essential role of ATG16L1 in autophagy regulation (Fig. 6I). Collectively, these findings demonstrate that KDM5B binds to ATG16L1 and interferes with the assembly of the ATG12-ATG5-ATG16L1 complex, thereby impairing autophagosome maturation and contributing to the progression of ALI.

Knockdown of KDM5B inhibited the cGAS-STING/NF-κB signaling pathways in ALI

To further investigate the role of KDM5B in regulating autophagy and inflammation during ALI, we analyzed its connection to the cGAS-STING and NF-κB signaling pathways, both of which are central mediators of immune-inflammatory responses. Gene Set Enrichment Analysis (GSEA) revealed significant activation of the cytosolic DNA-sensing and NF-κB signaling pathways in CCl_4-induced ALI,

implicating their involvement in disease progression (Fig. 7A-B). Western blotting demonstrated that LPS treatment markedly increased the expression of cGAS and enhanced the phosphorylation of STING, TBK1, IRF3, and NF-κB p65, indicating strong activation of inflammatory signaling pathways. Notably, knockdown of KDM5B significantly suppressed this activation (Fig. 7C). Confocal laser scanning microscopy further confirmed these findings, showing that KDM5B knockdown significantly attenuated LPS-induced levels of phosphorylated STING, TBK1, and IRF3 (Fig. 7D). Taken together, these results demonstrate that KDM5B knockdown attenuates activation of the cGAS-STING pathway and downstream NF-κB signaling, thereby reducing inflammatory cytokine production and mitigating the progression of ALI.

Discussion

This study identified a significant upregulation of KDM5B in CCl_4-induced ALI and uncovered a novel pathogenic mechanism. Mechanistically, KDM5B binds to ATG16L1 and disrupts the formation of the ATG12-ATG5-ATG16L1 complex, impairing autophagosome maturation. This autophagy dysfunction leads to cytosolic DNA accumulation, activating the cGAS-STING signaling pathway and promoting excessive release of inflammatory mediators, thereby aggravating hepatic injury. These findings highlight KDM5B as a critical regulator of ALI and propose it as a potential molecular target for therapeutic intervention (Fig. 8).

Emerging evidence has linked KDM5B to the progression of multiple hepatic diseases, including the promotion of tumorigenesis in hepatocellular carcinoma [31] and facilitation of fibrosis in alcoholic liver disease [32]. However, its role in ALI remained undefined. Through integrated bioinformatics and experimental validation, we found that KDM5B was markedly upregulated in CCl_4-induced ALI and that its knockdown significantly alleviated liver injury, establishing KDM5B as a central driver of ALI pathogenesis.

Immune cell infiltration and sustained inflammation are hallmark features of ALI [33]. Hepatocytes respond to injury by secreting type I interferon (IFN-β) [34], which subsequently activates downstream interferon-stimulated genes (e.g., ISG15, contributing to immune modulation [35]. IFN-β also promotes the expression of chemokines like CXCL10, which recruits $CD11b^+$ myeloid cells to the liver, where they differentiate into $F4/80^+$ macrophages [36]. These infiltrating macrophages amplify inflammation by releasing large quantities of pro-inflammatory cytokines, thus exacerbating liver damage [37]. Although the inflammatory pathways in ALI are well-documented, the upstream regulatory mechanisms remain poorly understood. Our findings demonstrated increased hepatic infiltration of $CD11b^+F4/80^+$ macrophages and elevated expression of CXCL10, ISG15, IFN-β, and key pro-inflammatory cytokines in ALI. Importantly, liver-specific knockdown of KDM5B significantly reduced macrophage infiltration and suppressed the expression of these inflammatory mediators. Collectively, this study revealed that KDM5B aggravated liver injury by impairing autophagy and enhancing immune cell recruitment and

inflammatory cytokine production, thereby offering new insights into the molecular mechanisms of ALI and a promising therapeutic target.

Autophagy is an essential cellular process that maintains homeostasis at both the cellular and organismal levels [38]. This multistep process is initiated by autophagosome formation, which is primarily regulated by members of the autophagy-related protein family [39]. Among them, ATG16L1 binds to the ATG12-ATG5 conjugate to form the ATG12-ATG5-ATG16L1 complex, which is critical for catalyzing LC3 lipidation and driving autophagosome maturation [40]. Recent studies have highlighted the role of epigenetic regulators, particularly histone-modifying enzymes, in modulating autophagy in liver diseases [41]. For instance, Wang *et al.* [42] reported that inhibition of the histone demethylase KDM8 activates autophagy and suppresses hepatocellular carcinoma growth. In line with this, our study identified KDM5B as another histone demethylase regulating autophagy in the context of ALI. Notably, KDM5B knockdown restored autophagic flux, as indicated by an increased LC3-II/LC3-I ratio, elevated Beclin-1 expression, and reduced accumulation of the autophagy substrate p62/SQSTM1. Importantly, we further demonstrated that KDM5B directly interacted with ATG16L1, disrupting the assembly of the ATG12-ATG5-ATG16L1 complex. This interference impaired LC3 lipidation, reduced autophagosome biogenesis, and ultimately inhibited autophagic flux.

To explore the role of KDM5B in regulating inflammation during ALI, we performed GSEA, which revealed significant enrichment of the cGAS-STING and NF-κB signaling pathways. Notably, the cGAS-STING axis is pivotal for hepatic inflammatory responses by sensing cytosolic DNA and generating cGAMP, thereby activating TBK1[43, 44]. Activated TBK1 subsequently phosphorylates key components of the NF-κB signaling pathway [45], leading to the transcription of pro-inflammatory genes expression. Our findings demonstrated that knockdown of KDM5B suppressed activation of the cGAS-STING pathway in macrophages, as evidenced by reduced phosphorylation of STING, TBK1, IRF3, and NF-κB p65. This attenuation of signaling results in dampened downstream inflammatory responses. Collectively, these results reveal a clear mechanistic link between KDM5B and the activation of cGAS-STING/NF-κB mediated inflammation in ALI.

Collectively, this study established KDM5B as a critical modulator of ALI pathogenesis, mechanistically linking its regulation of autophagy and inflammatory signaling to CCl_4-induced liver injury. However, further investigation is required to elucidate the role of KDM5B across different pathological stages and its interactions with additional signaling pathways. This will be essential to fully define the functional landscape of KDM5B in ALI and to strengthen the molecular foundation for developing targeted therapeutic strategies.

Conclusion

In summary, our study identified KDM5B as a pivotal regulator of ALI. Mechanistically, KDM5B bound to ATG16L1 and disrupted the formation of the ATG12-ATG5-ATG16L1 complex, thereby impairing LC3 lipidation and autophagosome maturation. This autophagy defect led to cytoplasmic DNA accumulation,

which activated the cGAS-STING-TBK1/NF-κB signaling axis. Therefore, $CD11b^{+}F4/80^{+}$ macrophages were recruited to the liver, and pro-inflammatory cytokines, including IL-6, IL-1β, IL-18, TNF-α, and CXCL10, were released, amplifying the inflammatory response and exacerbating ALI pathology. These findings not only elucidate a novel mechanism underlying ALI progression but also highlight the KDM5B-ATG16L1 axis as a promising therapeutic target for the treatment of ALI.

Methods

Animal model establishment and experimental procedures

The 6-8-week-old male C57BL/6J mice were supplied by Wuhan Mouse Bailey Biotechnology Co., Ltd (Wuhan, China). Animals were housed under strictly controlled conditions at 20–22°C with 40–70% humidity. The experimental group was injected with adeno-associated virus AAV-shKDM5B or AAV8-KDM5B via the tail vein. Following a two-weeks period to ensure sufficient viral expression, ALI was induced via intraperitoneal administration of CCl_4 (1 mL/kg). Right before the injection, CCl_4 was meticulously diluted in olive oil (1:10, v/v) and aseptically filtered through 0.22 μm membranes. Hepatic tissues were harvested 24 hours post-induction. All study protocols were received approval from the Laboratory Animal Ethics Committee of Hubei Institute of Science and Technology.

Hematoxylin-eosin (H&E) staining

Murine liver tissues were fixed in 4% paraformaldehyde. Following fixation, the tissues were dehydrated through an ascending ethanol gradient series. Subsequently, the tissues were embedded in paraffin and sectioned at 5 μm. The sections were then stained with H&E. Histopathological alterations in the liver tissues were assessed using light microscopy.

Immunohistochemistry

Following fixation, liver tissues were paraffin-embedded, sectioned, dewaxed, and rehydrated. Antigen retrieval was performed using heated citric acid buffer (10 mM, pH 6.0). To quench endogenous peroxidase activity, tissue sections were treated with 3% hydrogen peroxide for 10 minutes. Nonspecific binding sites were blocked with 5% bovine serum albumin (BSA). Sections were then incubated with primary antibodies and maintained at 4°C overnight. The following day, matched secondary antibodies were applied, and incubation proceeded for 2 hours at ambient temperature. DAB chromogenic substrate was then applied, followed by hematoxylin counterstaining. Sections were permanently mounted with coverslips and examined under a light microscope.

Isolation of primary hepatocytes

Primary hepatocytes were isolated from C57BL/6J mice. After anesthesia was induced with 35% chloral hydrate, a thoracotomy was performed to expose the portal vein. Cannulation of the portal vein and inferior vena cava was established using indwelling needles. The liver was sequentially perfused with 25 mL calcium-free perfusion buffer followed by 0.05% collagenase IV solution (Worthington, LS004188). Enzymatic digestion was terminated when the liver exhibited softening, collapse, and persistent finger-pressure indentation. Following digestion, the liver was placed in a dish containing serum-free DMEM supplemented with 1% penicillin-streptomycin. After removing the Glisson's capsule, hepatocytes were released by gentle agitation and filtered through a 100-mesh sterile sieve (Biosharp, China). The cell suspension underwent multiple cycles of centrifugation (400× g, 3 minutes, 4°C) with washing and resuspension steps. Viable hepatocytes were finally resuspended in complete DMEM medium, counted, and plated.

Transcriptome RNA sequencing

Collected mouse liver tissues underwent homogenization in RNAiso Plus (Takara, Tokyo, Japan), followed by total RNA isolation. The KAPA mRNA-Seq Kit was utilized to generate sequencing libraries, processed samples underwent paired-end sequencing on an Illumina HiSeq X instrument. The resulting reads were mapped to the murine reference genome (GRCm39) using TopHat. DESeq2 was employed for the quantification and normalization of transcript-level read counts, enabling the identification of differentially expressed genes (DEGs).

Cell culture and transfection procedure

The murine hepatocyte line AML12 was commercially acquired from the ATCC (Manassas, VA, USA). RAW264.7 cells were obtained from Procell company (Wuhan, China). Cells were cultured in standard DMEM containing 10% FBS and 1% penicillin-streptomycin at 37°C within a 5% CO_2 humidified environment. Plasmids encoding shKDM5B were transfected into cells using the Neofect™ Transfection Reagent (Beijing, China) according to the manufacturer's protocol. After a 24-hours incubation, cells were exposed to 1 μg/mL LPS for 24 hours before being harvested.

RNA extraction and real-time PCR

Total RNA was extracted from liver tissues or cultured cells, respectively, using TRIzol Reagent (Thermo Fisher Scientific) following the manufacturer’s instructions. Subsequently, complementary DNA (cDNA) was synthesized from total RNA (1 μg) via the HiScript III RT SuperMix for qPCR kit (Vazyme, China). Amplification of quantitative PCR products was carried out employing the SYBR Green qPCR Master Mix (Vazyme, China) on a real-time thermocycler. Relative quantification of target genes was performed, with normalization against GAPDH and subsequent calculation by $2^{-\Delta\Delta Ct}$ analysis. Amplification primer sequences are listed in Table S1.

Western blotting Analysis

From liver specimens or cell cultures, proteins were isolated utilizing RIPA lysis buffer. Subsequently, total protein quantification was performed using a BCA assay kit. Protein lysates were resolved on 12% SDS-PAGE gels and electrotransferred to PVDF membranes. Membranes were blocked with 5% skim milk for 1 hour at room temperature. Next, primary antibody incubation proceeded overnight at 4°C. Following three washes in TBST, membranes were incubated with secondary antibodies at room temperature for 1 h. Following comprehensive rinsing with TBST, the proteins were detected using an ECL substrate kit (Biosharp, China) and documented by ImageQuant LAS 500 chemiluminescence imaging system (Cytiva, USA). Lastly, signal intensities were processed via ImageJ software (NIH, USA). Details of the primary antibodies are listed in Table S2.

Isolation and Flow Cytometric Profiling of Hepatic Macrophages

Small fragments were prepared from liver tissues and digested using RPMI 1640 medium containing 0.05% collagenase IV (Roche) and 0.01% trypsin inhibitor (Gibco, Thermo Fisher Scientific) at 37°C for 60 minutes. The tissue digest was filtered through a 40-μm cell strainer. Subsequently, the generated single-cell suspension underwent centrifugation, with the supernatant subsequently removed. Erythrocytes underwent hypotonic lysis, followed by centrifugation (800×g, 10 minutes, 4°C). The isolated cells were then resuspended in 40% Percoll and subjected to centrifugation at 2,000 rpm for 30 minutes. After aspiration of the supernatant fluid, the cell suspension was layered onto 80% Percoll gradient and centrifuged at ambient temperature. Subsequently, the pellet underwent two washing cycles, was resuspended in RPMI-1640 medium, and counted to achieve the desired cell density. Cells were then stained with anti-F4/80 (#123107, BioLegend) and anti-CD11b (#101211, BioLegend) antibodies in flow cytometry buffer for 45 minutes at 4°C in the dark. Analysis was performed using a flow cytometer with FlowJo software.

Transmission electron microscopy analysis

AML12 hepatocytes were fixed using 2.5% glutaraldehyde at 4°C for 2 hours, then subjected to 0.1 mol/L phosphate buffer. Post-fixation was performed utilizing 1% osmium tetroxide (OsO_4) for 2 hours. The cells were then dehydrated using a graded series of acetone and embedded in epoxy resin, polymerized, and sectioned. Ultrathin sections underwent double staining with 2% uranyl acetate and lead citrate, followed by examination of autophagosomes using transmission electron microscopy (HITA-CHI, Japan).

Immunofluorescence analysis

Cell specimens underwent fixation using 4% paraformaldehyde, permeabilization with Permeabilization Buffer (Servicebio, China), and blocking with 5% BSA (Biosharp, China). Following the blocking step, primary antibody incubation proceeded overnight at 4°C. Secondary antibodies and DAPI (Servicebio, China) were then added and incubated for 1 hour at room temperature in the dark. Imaging of the slides was performed using a laser scanning confocal microscope (Olympus FV3000), and ImageJ was applied for quantitative analysis of the images.

Immunoprecipitation

AML12 cells were lysed with IP lysis buffer (Beyotime, China) containing a protease inhibitor mix (ABclonal, China) over ice for 30 minutes. Following this, lysates were processed by centrifugation (12000× g, 15 minutes, 4°C), after which the supernatants were collected. Cell lysates were immunoprecipitated with specific antibodies overnight at 4°C. After that, Protein A/G magnetic beads were mixed with the lysates for 4 hours at 4°C to capture immunocomplexes. Finally, bound proteins were then eluted by boiling in loading buffer for 10 minutes at 100°C, followed by immunoblotting analysis.

Mass Spectrometry Analysis of Hepatocytes

Lysis of AML12 cells was performed on ice for 30 minutes with 500 μL pre-chilled IP lysis buffer. This buffer consisted of 50 mM Tris-HCl (pH 7.4), 150 mM NaCl, 1% NP-40, and 0.5% sodium deoxycholate, and was supplemented with cocktails of protease and phosphatase inhibitors. Following lysis, the supernatant was incubated overnight at 4°C with 2 μg of anti-KDM5B antibody or cognate IgG control. Subsequently, pre-washed Protein A/G agarose beads were added to the antigen-antibody mixture and following a 4-hours rotation incubation at 4°C, beads were pelleted via brief centrifugation (1,000× g, 1 min). The bead-bound immunocomplexes were next washed thrice using ice-cold TBST buffer. Following the final wash, the beads were resuspended in 2× loading buffer and subjected to heat denaturation at 100°C for 10 minutes. The eluted proteins were subsequently resolved on SDS-PAGE gels. Post-electrophoresis, the gel band corresponding to the sample was excised. The extracted peptides underwent analysis via liquid chromatography-tandem mass spectrometry (LC-MS/MS). The MS/MS spectra obtained were searched against the mouse non-redundant protein database (NCBI), utilizing the Mascot algorithm from Matrix Science.

Statistical analysis

Statistical evaluations were conducted using GraphPad Prism version 9.0. Results are presented as mean ± SEM, derived from a minimum of three separate experiments. Differences between groups were assessed using one-way ANOVA, and subsequent multiple comparisons were performed using two-way

ANOVA with Tukey's test. Statistical significance is indicated as *P < 0.05, **P < 0.01, ***P < 0.001; n.s. represents non-significant results.

Declarations

Author contributions

L.Q. and C.C. conceived and designed the study, including determining the core direction and experimental protocols. H.O. and Y.M. performed the in vivo and in vitro experiments, and drafted the manuscript with the assistance of other co-authors. J.X. and Q.Y. curated the data using statistical software and analytical methods. W.H. and X.Q. conducted the literature search and organized the references. J.W., D.L., X.Q., Y.B. and S.S. revised the language of the first draft. All the authors reviewed every aspect of the manuscript and approved the version as submitted.

Funding

This article was supported by the National Natural Science Foundation of China (No. 82302365), Natural Science Foundation of Hubei Province, China (No. 2024AFB517), Hubei University of Science and Technology Development Fund Project (No. BK202442) and Foundation of Hubei University of Science and Technology Science “Special Project on Diabetes and Angiopathy” (No.2024TNB05).

Competing interests

The authors declare no conflicts of interest.

References

1. Asrani SK, Devarbhavi H, Eaton J, Kamath PS. Burden of liver diseases in the world. *J Hepatol* 2019, **70**(1)**:** 151-171.
2. Stravitz RT, Lee WM. Acute liver failure. *Lancet* 2019, **394**(10201)**:** 869-881.
3. Bernal W, Auzinger G, Dhawan A, Wendon J. Acute liver failure. *Lancet* 2010, **376**(9736)**:** 190-201.
4. Chung RT, Stravitz RT, Fontana RJ, Schiodt FV, Mehal WZ, Reddy KR*, et al.* Pathogenesis of liver injury in acute liver failure. *Gastroenterology* 2012, **143**(3)**:** e1-e7.
5. Zuo J, Tian YX, An Q, Wu BY, Yang JR, Fan YC. Potential Biomarkers and Therapeutic Targets in Hepatitis B Virus-related Acute Liver Failure: Interplay of the Ferroptosis, Autophagy and Immune Responses. *Int J Med Sci* 2025, **22**(4)**:** 806-818.
6. Nguyen GC, Sam J, Thuluvath PJ. Hepatitis C is a predictor of acute liver injury among hospitalizations for acetaminophen overdose in the United States: a nationwide analysis. *Hepatology* 2008, **48**(4)**:** 1336-1341.
7. Yu Q, Zhang J, Li J, Song Y, Pan J, Mei C*, et al.* Sirtuin 5-Mediated Desuccinylation of ALDH2 Alleviates Mitochondrial Oxidative Stress Following Acetaminophen-Induced Acute Liver Injury. *Adv*

Sci (Weinh) 2024, **11**(39)**:** e2402710.

8. Luo K, Jahufer MZ, Wu F, Di H, Zhang D, Meng X*, et al.* Genotypic Variation in a Breeding Population of Yellow Sweet Clover (Melilotus officinalis). *Front Plant Sci* 2016, **7:** 972.
9. Fernández J, Bassegoda O, Toapanta D, Bernal W. Acute liver failure: A practical update. *JHEP Rep* 2024, **6**(9)**:** 101131.
10. Hill AL, Khan M, Kiani AZ, Lindemann JD, Vachharajani N, Doyle MB*, et al.* Global liver transplantation: emerging trends and ethical challenges. *Langenbecks Arch Surg* 2023, **408**(1)**:** 418.
11. Amjad W, Thuluvath P, Mansoor M, Dutta A, Ali F, Qureshi W. N-acetylcysteine in non-acetaminophen-induced acute liver failure: a systematic review and meta-analysis of prospective studies. *Prz Gastroenterol* 2022, **17**(1)**:** 9-16.
12. Liu S, Yao S, Yang H, Liu S, Wang Y. Autophagy: Regulator of cell death. *Cell Death Dis* 2023, **14**(10)**:** 648.
13. Xia F, Li W, Wang W, Liu J, Li X, Cai J*, et al.* S-palmitoylation coordinates the trafficking of ATG9A to mediate autophagy initiation. *Autophagy* 2025**:** 1-21.
14. Magné J, Green DR. LC3-associated endocytosis and the functions of Rubicon and ATG16L1. *Sci Adv* 2022, **8**(43)**:** eabo5600.
15. Mizushima N, Komatsu M. Autophagy: renovation of cells and tissues. *Cell* 2011, **147**(4)**:** 728-741.
16. Zhan X, Bai Y, Zhu Q, Gao Y, Li F, Bu Q*, et al.* Macrophage ATG16L1 promotes liver regeneration after partial hepatectomy. *JHEP Rep* 2025, **7**(5)**:** 101330.
17. Ilyas G, Zhao E, Liu K, Lin Y, Tesfa L, Tanaka KE*, et al.* Macrophage autophagy limits acute toxic liver injury in mice through down regulation of interleukin-1β. *J Hepatol* 2016, **64**(1)**:** 118-127.
18. Matoba K, Noda NN. Structural catalog of core Atg proteins opens new era of autophagy research. *J Biochem* 2021, **169**(5)**:** 517-525.
19. Yamamoto H, Zhang S, Mizushima N. Autophagy genes in biology and disease. *Nat Rev Genet* 2023, **24**(6)**:** 382-400.
20. Hui S, Kan W, Qin S, He P, Zhao J, Li H*, et al.* Glycyrrhiza uralensis polysaccharides ameliorates cecal ligation and puncture-induced sepsis by inhibiting the cGAS-STING signaling pathway. *Front Pharmacol* 2024, **15:** 1374179.
21. Wen J, Qin S, Li Y, Zhang P, Zhan X, Fang M*, et al.* Flavonoids derived from licorice suppress LPS-induced acute lung injury in mice by inhibiting the cGAS-STING signaling pathway. *Food Chem Toxicol* 2023, **175:** 113732.
22. Shen M, Jiang X, Peng Q, Oyang L, Ren Z, Wang J*, et al.* The cGAS–STING pathway in cancer immunity: mechanisms, challenges, and therapeutic implications. *J Hematol Oncol* 2025, **18**(1)**:** 40.
23. Luo W, Song Z, Xu G, Wang H, Mu W, Wen J*, et al.* LicochalconeB inhibits cGAS-STING signaling pathway and prevents autoimmunity diseases. *Int Immunopharmacol* 2024, **128:** 111550.
24. Decout A, Katz JD, Venkatraman S, Ablasser A. The cGAS-STING pathway as a therapeutic target in inflammatory diseases. *Nat Rev Immunol* 2021, **21**(9)**:** 548-569.

25. Li XJ, Qu JR, Zhang YH, Liu RP. The dual function of cGAS-STING signaling axis in liver diseases. *Acta Pharmacol Sin* 2024, **45**(6)**:** 1115-1129.
26. Liu Z, Wang M, Wang X, Bu Q, Wang Q, Su W*, et al.* XBP1 deficiency promotes hepatocyte pyroptosis by impairing mitophagy to activate mtDNA-cGAS-STING signaling in macrophages during acute liver injury. *Redox Biol* 2022, **52:** 102305.
27. Klein BJ, Piao L, Xi Y, Rincon-Arano H, Rothbart SB, Peng D*, et al.* The histone-H3K4-specific demethylase KDM5B binds to its substrate and product through distinct PHD fingers. *Cell Rep* 2014, **6**(2)**:** 325-335.
28. Schonfeld M, Averilla J, Gunewardena S, Weinman SA, Tikhanovich I. Male-Specific Activation of Lysine Demethylases 5B and 5C Mediates Alcohol-Induced Liver Injury and Hepatocyte Dedifferentiation. *Hepatol Commun* 2022, **6**(6)**:** 1373-1391.
29. Zhang B, Li J, Wang Y, Liu X, Yang X, Liao Z*, et al.* Deubiquitinase USP7 stabilizes KDM5B and promotes tumor progression and cisplatin resistance in nasopharyngeal carcinoma through the ZBTB16/TOP2A axis. *Cell Death Differ* 2024, **31**(3)**:** 309-321.
30. Guo JC, Liu Z, Yang YJ, Guo M, Zhang JQ, Zheng JF. KDM5B promotes self-renewal of hepatocellular carcinoma cells through the microRNA-448-mediated YTHDF3/ITGA6 axis. *J Cell Mol Med* 2021, **25**(13)**:** 5949-5962.
31. Wang D, Han S, Peng R, Jiao C, Wang X, Yang X*, et al.* Depletion of histone demethylase KDM5B inhibits cell proliferation of hepatocellular carcinoma by regulation of cell cycle checkpoint proteins p15 and p27. *J Exp Clin Cancer Res* 2016, **35:** 37.
32. Schonfeld M, O'Neil M, Weinman SA, Tikhanovich I. Alcohol-induced epigenetic changes prevent fibrosis resolution after alcohol cessation in miceresolution. *Hepatology* 2024, **80**(1)**:** 119-135.
33. Hassan GS, Flores Molina M, Shoukry NH. The multifaceted role of macrophages during acute liver injury. *Front Immunol* 2023, **14:** 1237042.
34. Bolen CR, Ding S, Robek MD, Kleinstein SH. Dynamic expression profiling of type I and type III interferon-stimulated hepatocytes reveals a stable hierarchy of gene expression. *Hepatology* 2014, **59**(4)**:** 1262-1272.
35. Perng YC, Lenschow DJ. ISG15 in antiviral immunity and beyond. *Nat Rev Microbiol* 2018, **16**(7)**:** 423-439.
36. Ju C, Tacke F. Hepatic macrophages in homeostasis and liver diseases: from pathogenesis to novel therapeutic strategies. *Cell Mol Immunol* 2016, **13**(3)**:** 316-327.
37. Barbier L, Ferhat M, Salamé E, Robin A, Herbelin A, Gombert JM*, et al.* Interleukin-1 Family Cytokines: Keystones in Liver Inflammatory Diseases. *Front Immunol* 2019, **10:** 2014.
38. Klionsky DJ, Petroni G, Amaravadi RK, Baehrecke EH, Ballabio A, Boya P*, et al.* Autophagy in major human diseases. *Embo j* 2021, **40**(19)**:** e108863.
39. Nakatogawa H. Mechanisms governing autophagosome biogenesis. *Nat Rev Mol Cell Biol* 2020, **21**(8)**:** 439-458.

40. Wei F, Wang Y, Yao J, Mei L, Huang X, Kong H*, et al.* ZDHHC7-mediated S-palmitoylation of ATG16L1 facilitates LC3 lipidation and autophagosome formation. *Autophagy* 2024, **20**(12)**:** 2719-2737.
41. Shu F, Xiao H, Li QN, Ren XS, Liu ZG, Hu BW*, et al.* Epigenetic and post-translational modifications in autophagy: biological functions and therapeutic targets. *Signal Transduct Target Ther* 2023, **8**(1)**:** 32.
42. Wang L, Shi R, Wang S, Duan Y, Wang Z, Zheng P*, et al.* ADSL promotes autophagy and tumor growth through fumarate-mediated Beclin1 dimethylation. *Nat Chem Biol* 2025**, 21**(6)**:** 894-905.
43. Chen R, Du J, Zhu H, Ling Q. The role of cGAS-STING signalling in liver diseases. *JHEP Rep* 2021, **3**(5)**:** 100324.
44. Xu D, Tian Y, Xia Q, Ke B. The cGAS-STING Pathway: Novel Perspectives in Liver Diseases. *Front Immunol* 2021, **12:** 682736.
45. Zhang L, Wei X, Wang Z, Liu P, Hou Y, Xu Y*, et al.* NF-κB activation enhances STING signaling by altering microtubule-mediated STING trafficking. *Cell Rep* 2023, **42**(3)**:** 112185.

Figures

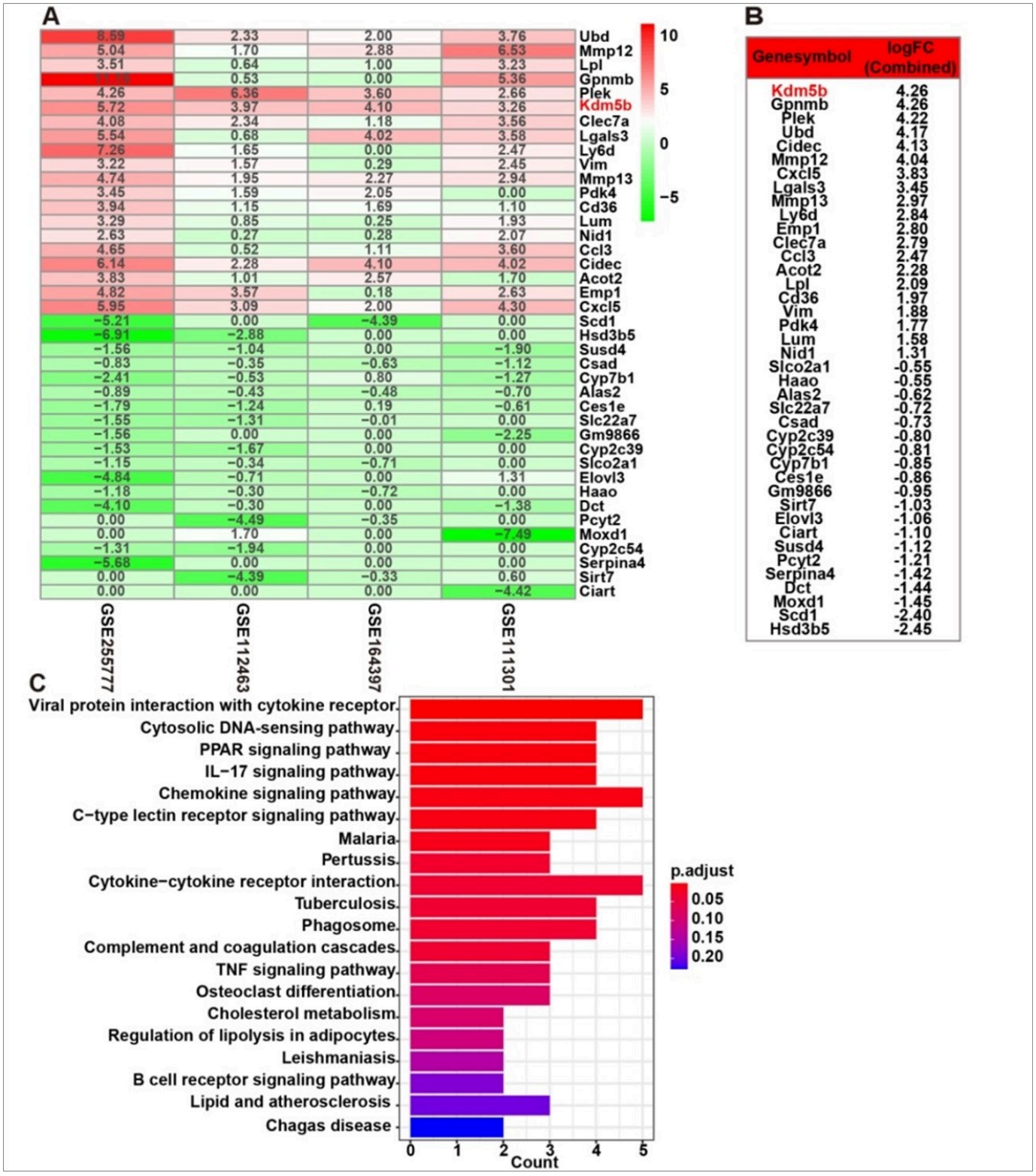


Figure 1

Bioinformatics Analysis of Four ALI Datasets and KEGG Analysis. A Heatmap analysis of 40 significantly differentially expressed genes between ALI patients and normal controls. Red indicates upregulation and green indicates downregulation. **B** The log2 FC of 40 DEGs was calculated based on RRA of the 4 datasets. **C**KEGG enrichment analysis of key pathways in the integrated dataset.

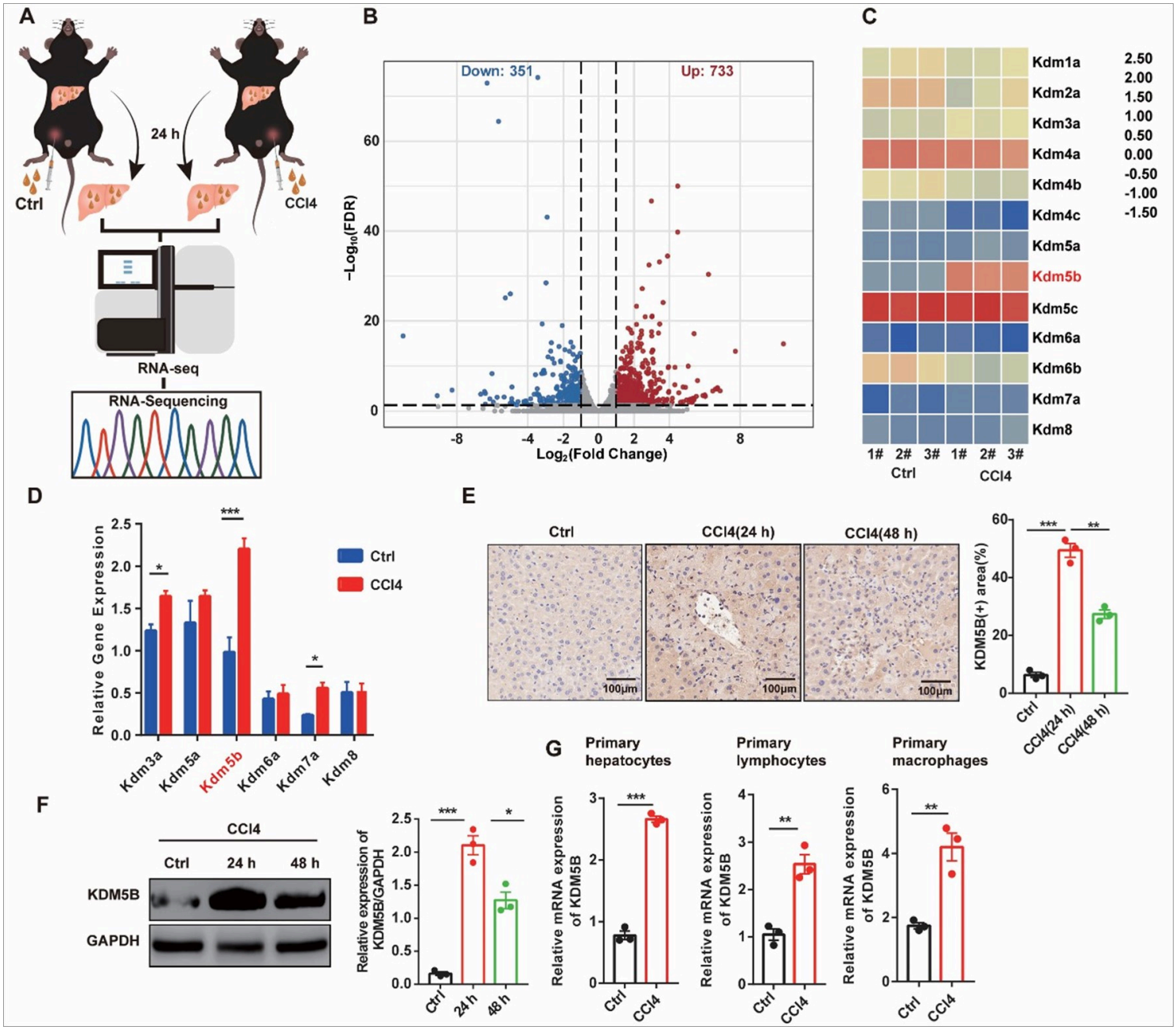


Figure 2

Validation of KDM5B expression in CCl_4-induced ALI mouse model. A Schematic diagram of the experiment in which mice were constructed as an ALI model by intraperitoneal injection of CCl_4 and liver tissues were obtained for RNA-seq after 24 hours. **B** Volcano plot of differentially expressed mRNAs between control and CCl_4-induced mice. Red marks upregulated genes, and blue marks downregulated genes. **C** Heatmap analysis of KDM family gene expression patterns in control and CCl_4-induced ALI mice. **D** qRT-PCR analysis of KDM family gene expression in control and CCl_4-induced ALI mice. **E-F** Immunohistochemistry and western blotting analysis of KDM5B levels in hepatic tissues of CCl_4-induced mice at distinct time points. **G** qRT-PCR was used to assess the levels of KDM5B mRNA in primary

hepatocytes, lymphocytes, and macrophages of CCl_4-induced mice, respectively. Results displayed as mean ± SEM (n = 3; *P < 0.05, **P < 0.01, ***P < 0.001).

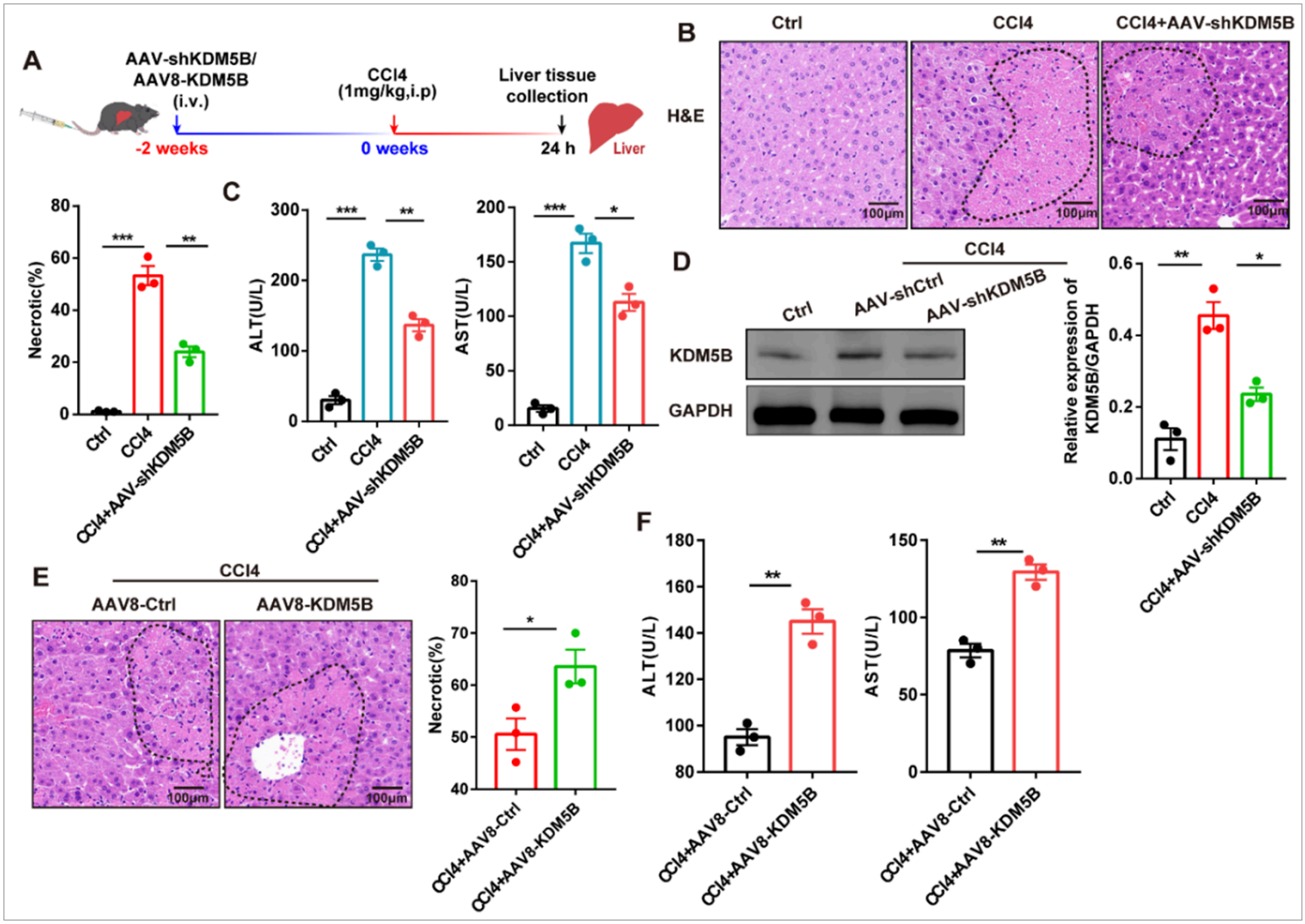


Figure 3

KDM5B knockdown attenuates while its overexpression exacerbates CCl_4-induced ALI. A Flow chart of the experiment: tail vein injection of AAV-shKDM5B or AAV8-KDM5B adeno-associated virus was performed, followed by intraperitoneal CCl_4 administration (1 mL/kg) after 2 weeks, and livers were harvested at 24 hours post-induction. **B** H&E staining showing pathological changes in liver morphology across different groups (scale bar = 100 μm). The graph depicts quantitative analysis of the necrotic area. **C** Measurement of serum ALT and AST levels in various mouse groups. **D** Western blotting detection and quantitation of hepatic KDM5B in AAV-shKDM5B-treated mice. **E-F** H&E-stained liver sections (scale bar = 100 μm) with serum ALT and AST measurement in AAV8-KDM5B mice. Results displayed as mean ± SEM (n = 3; *P < 0.05, **P < 0.01, ***P < 0.001).

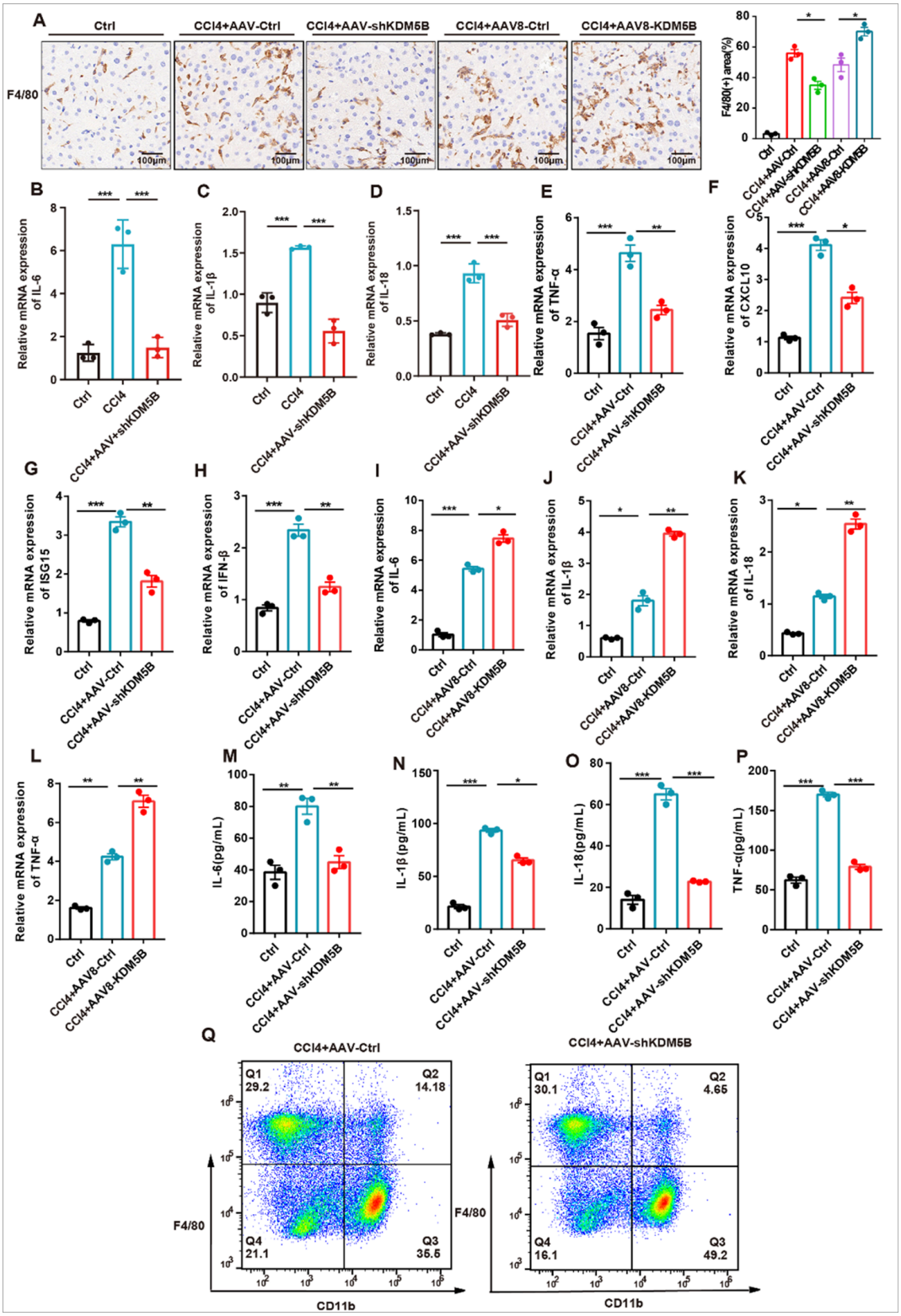


Figure 4

Knockdown of KDM5B attenuates the inflammatory response to CCl_4-induced ALI in mice. A Immunohistochemistry staining for F4/80$^+$ macrophages in mouse liver tissues (scale bar = 100 μm). Quantification of macrophage infiltration is shown on the right. **B-H** qRT-PCR analysis of IL-6, IL-1β, IL-18, TNF-α, CXCL10, ISG15, and IFN-β mRNA expression in hepatic tissues of AAV-shKDM5B mice compared to control groups. **I-L** qRT-PCR analysis of IL-6, IL-1β, IL-18, TNF-α mRNA expression in hepatic tissues of

AAV8-KDM5B mice compared to control groups. **M-P** ELISA analysis of serum levels of inflammatory cytokines IL-6, IL-1β, IL-18, and TNF-α in AAV-shKDM5B mice compared to control groups. **Q** Flow cytometry analysis of $CD11b^{+}F4/80^{+}$ macrophage population in liver tissues. Results displayed as mean ± SEM (n = 3; **P* < 0.05, ***P* < 0.01, ****P* < 0.001).

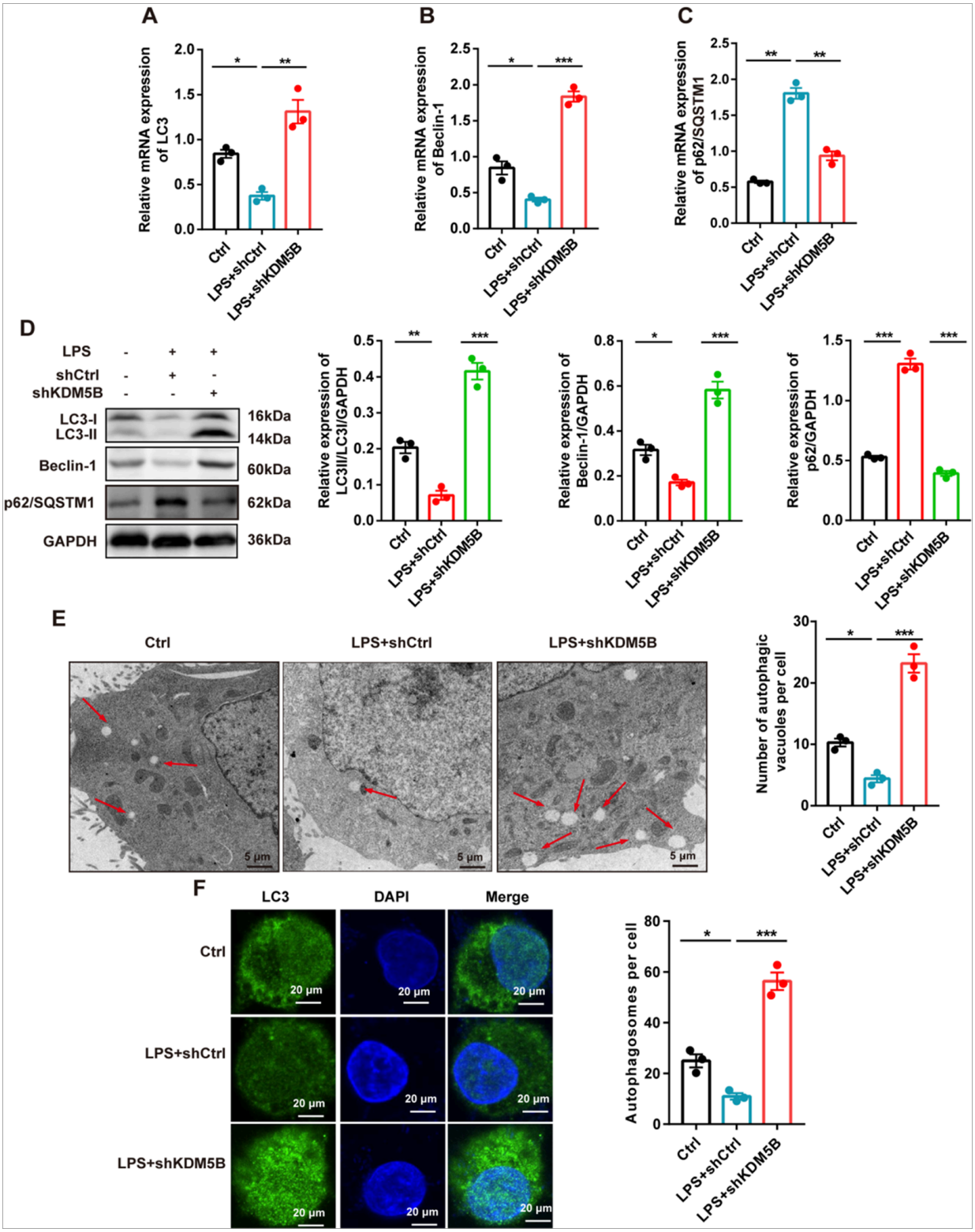


Figure 5

Knockdown of KDM5B ameliorates LPS-induced impairment of autophagy. A-C qRT-PCR was used to assess the mRNA levels of autophagy-related genes LC3, Beclin-1, and p62/SQSTM1 in AML12 cells. **D** Western blot analysis of LC3II/I, Beclin-1, and p62 protein levels in AML12 cells. **E** Transmission electron microscopy (TEM) observation of the morphology and number of autophagosomes in AML12 cells (scale bar = 5 μm), red arrows denote autophagosomes, and quantitative analysis of autophagosome number per cell is displayed on the right. **F** Laser confocal microscopy observation of LC3 expression in AML12 cells. Green fluorescence indicates autophagosomes (scale bar = 20 μm), with the number of autophagosomes per cell quantified on the right. Results displayed as mean ± SEM (n = 3; **P* < 0.05, ***P*< 0.01, ****P* < 0.001).

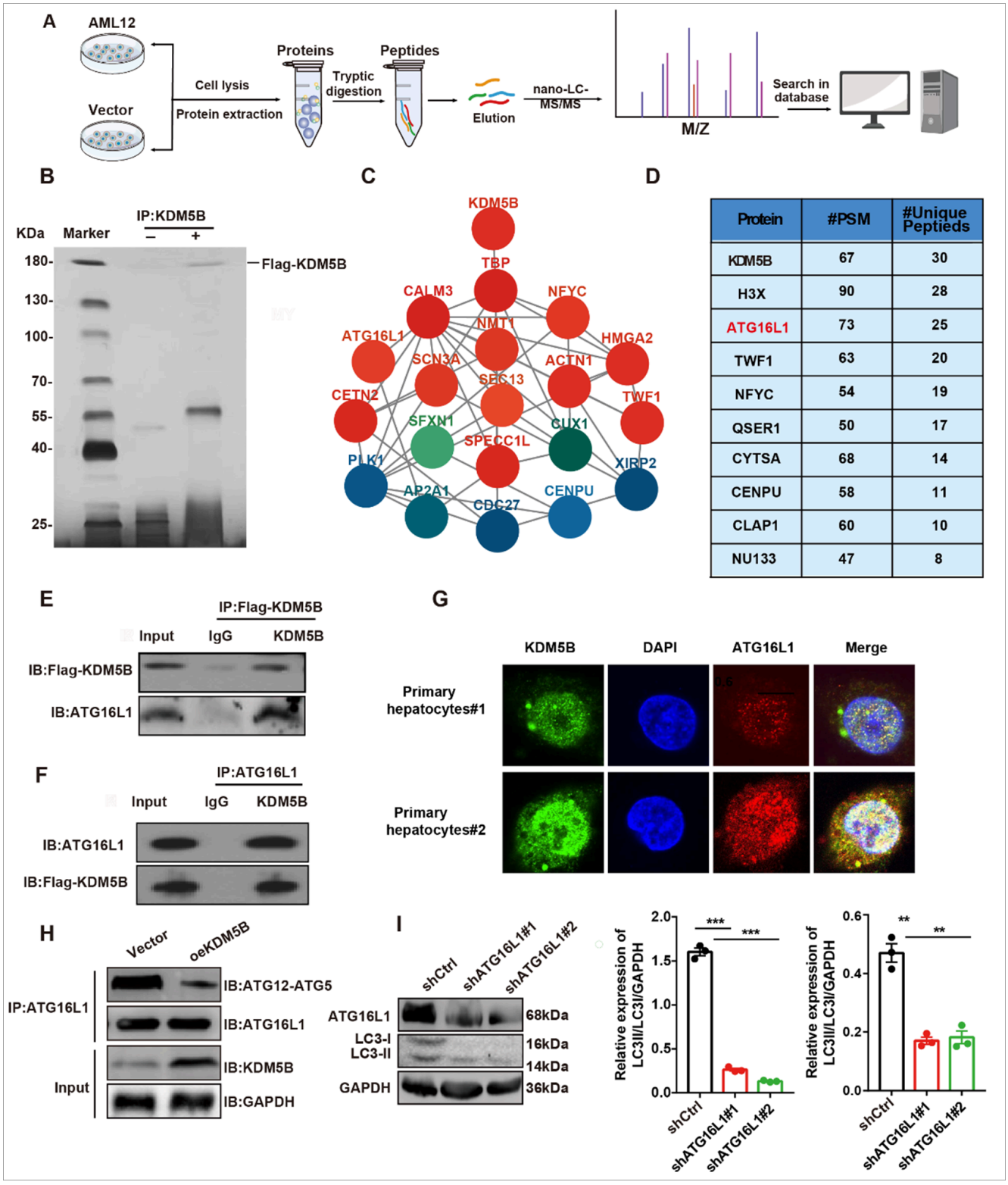


Figure 6

KDM5B binding to ATG16L1 impairs autophagy. A Schematic diagram of the process of constructing a cell line stably expressing Flag-KDM5B in AML12 cells, trypsin digestion followed by mass spectrometry analysis. **B**Silver staining experiments to validate Flag-KDM5B expression. **C**Construction of the KDM5B protein interaction network by STRING database. **D**Mass spectrometry identification of the top 10 KDM5B-interacting proteins. **E-F**Co-IP experiments confirming the interaction between KDM5B and

ATG16L1 from the perspective of KDM5B and ATG16L1, respectively. **G** Laser confocal microscopy was used to observe the co-localization of KDM5B and ATG16L1 in primary hepatocytes. **H** Overexpression of KDM5B in AML12 cell line was used to investigate how KDM5B overexpression affects the binding of ATG16L1 to the ATG12-ATG5 complex. **I** Knockdown of ATG16L1 was detected as a change in the level of the autophagy marker LC3II/I. Results displayed as mean ± SEM (n = 3; **P* < 0.05, ***P* < 0.01, ****P* < 0.001).

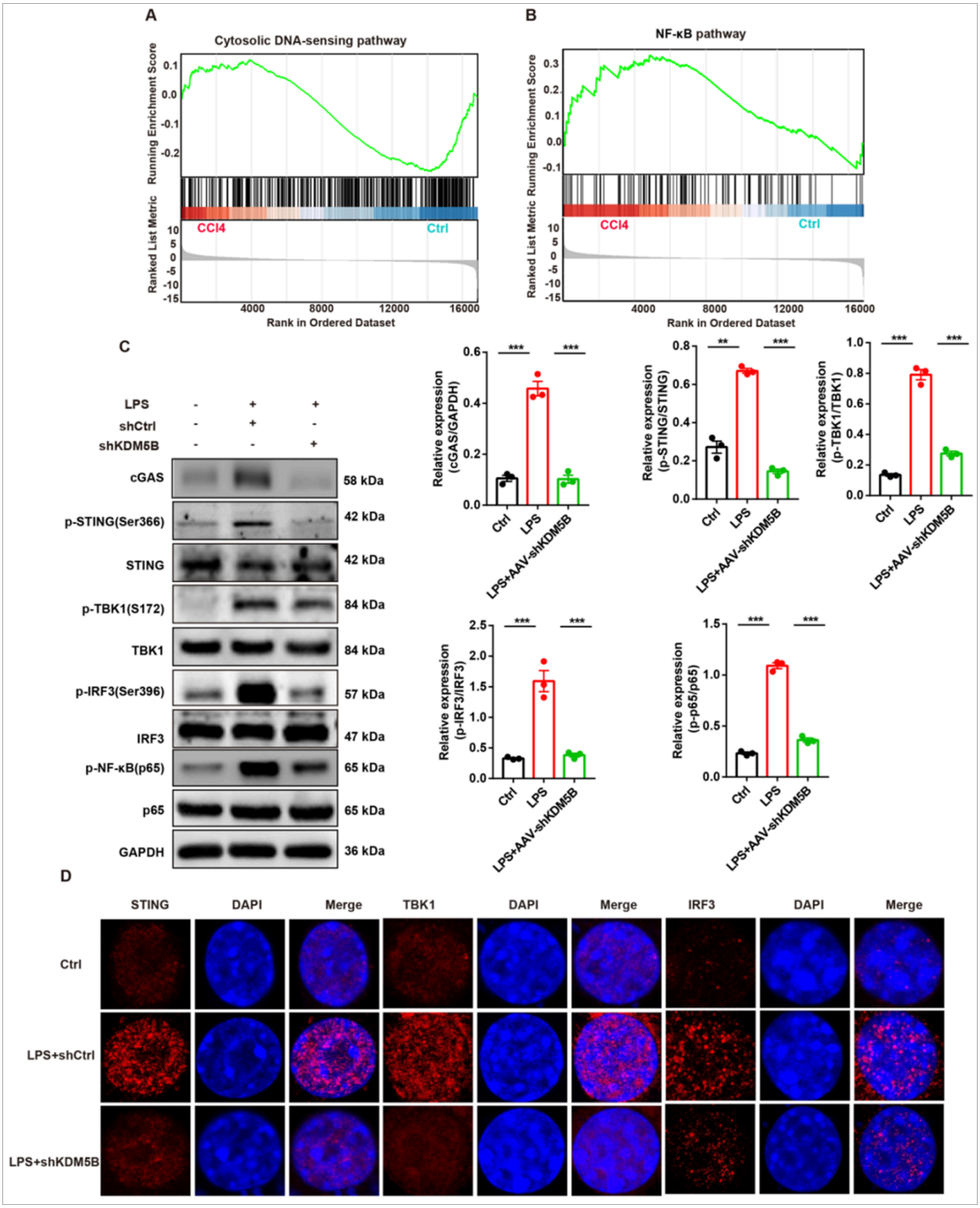


Figure 7

Effect of KDM5B on cGAS-STING and NF-κB signaling pathways. A-B GSEA showing the enrichment of cytoplasmic DNA-sensing pathway and NF-κB signaling pathway in CCl_4-induced ALI. **C** Western blotting analysis of cGAS, p-STING, STING, p-TBK1, TBK1, p-IRF3, IRF3, p-p65, and p65 protein expression in RAW264.7 macrophages. **D** Laser confocal microscopy to detect the expression levels of p-STING, p-TBK1 and p-IRF3 in RAW264.7 macrophages. (Nuclei stained with DAPI; target proteins shown in red. Scale bar = 20 μm). Results displayed as mean ± SEM (n = 3; **P* < 0.05, ***P* < 0.01, ****P* < 0.001).

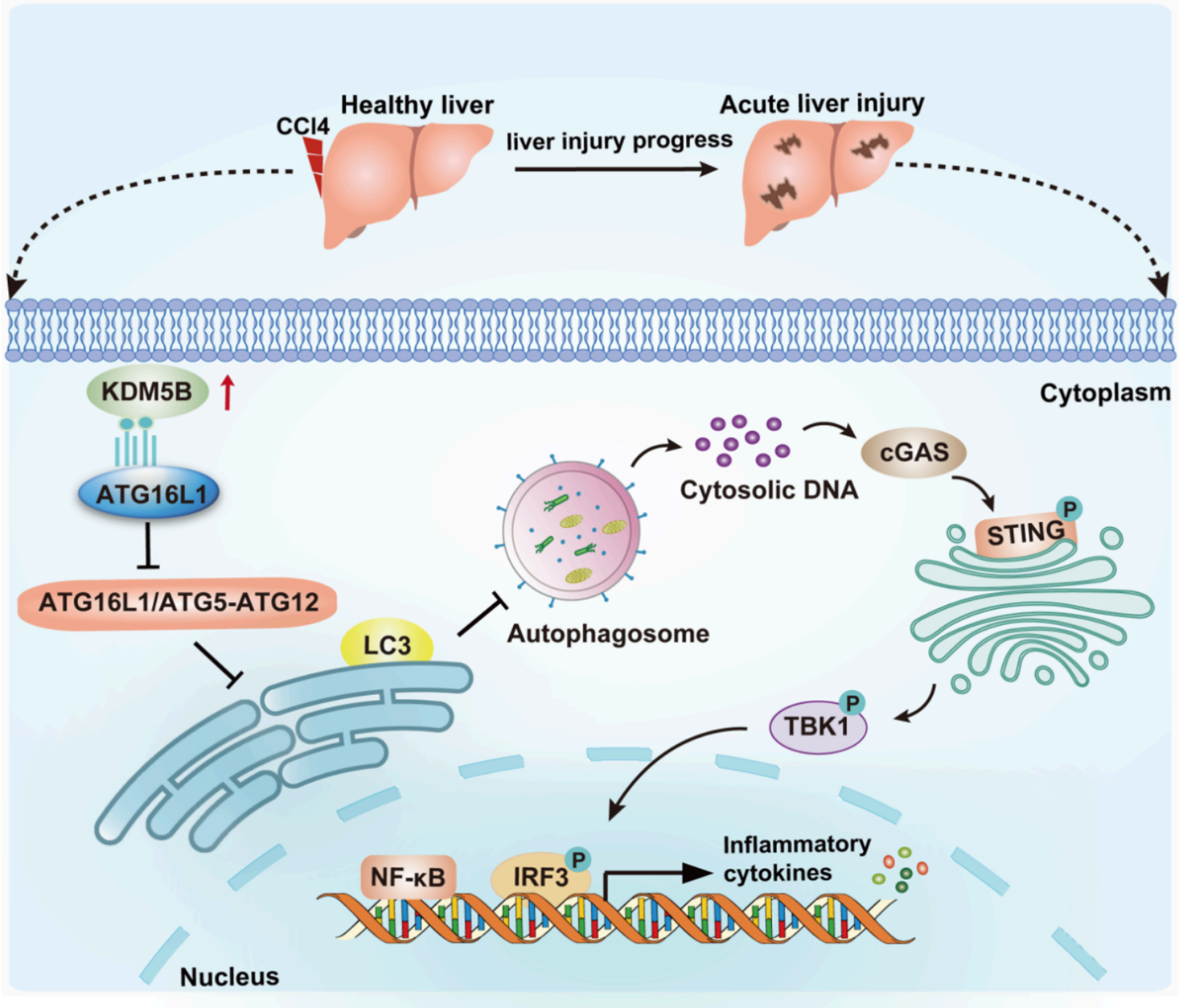


Figure 8

Molecular mechanism of KDM5B mediating autophagy and inflammation in ALI. In CCl_4-induced ALI, KDM5B expression is upregulated, and KDM5B binds to ATG16L1, disrupting the formation of ATG12-ATG5-ATG16L1 complex and inhibiting autophagosome maturation. This leads to cytoplasmic DNA accumulation and subsequent activation of the cGAS-STING cascade, which in turn evoked the generation of pro-inflammatory mediators and intensified hepatic injury.

Supplementary Files

This is a list of supplementary files associated with this preprint. Click to download.

- Figure1supplemental.xls
- Figure2supplemental.xlsx
- OriginalWesternblot.pdf
- TableS1.docx
- TableS2.docx